applied optics

Diffraction analysis for DMD-based scene projectors in the long-wave infrared

Qing Han,[1,2,*] Jianzhong Zhang,[1] Jian Wang,[1] and Qiang Sun[1]

[1]Changchun Institute of Optic, Fine Mechanics and Physics, Chinese Academy of Science, Changchun 130033, China
[2]University of Chinese Academy of Sciences, Beijing 100049, China
*Corresponding author: zheyuanhan@163.com

Received 12 July 2016; revised 5 September 2016; accepted 5 September 2016; posted 7 September 2016 (Doc. ID 269904); published 28 September 2016

Diffraction effects play a significant role in the digital micromirror device (DMD)-based scene projectors in the long-wave infrared (IR) band (8–12 μm). The contrast provided by these projector systems can become noticeably worse because of the diffraction characteristics of the DMD. We apply a diffraction grating model of the DMD based on the scalar diffraction theory and the Fourier transform to address this issue. In addition, a simulation calculation is conducted with MATLAB. Finally, the simulation result is verified with an experiment. The simulation and experimental results indicate that, when the incident azimuth angle is 0° and the zenith angle is between 42°and 46°, the scene projectors will have a good imaging contrast in the long-wave IR. The diffraction grating model proposed in this study provides a method to improve the contrast of DMD-based scene projectors in the long-wave IR.

OCIS codes: (260.1960) Diffraction theory; (050.1950) Diffraction gratings; (260.3060) Infrared; (070.2465) Finite analogs of Fourier transforms.

http://dx.doi.org/10.1364/AO.55.008016

1. INTRODUCTION

The infrared (IR) scene projector is a core part in IR scene simulation systems and provides IR target and background imaging in IR tracking systems. Research on IR scene simulation systems began in the 1970s, and a variety of IR scene projectors have been developed since then, including resistive arrays, laser diode arrays, IR liquid crystal light valves, and digital micromirror devices (DMDs) [1,2]. The DMD was invented by Texas Instruments in 1981 and was quickly used for IR scene projection. Moreover, DMD-based IR scene projectors developed rapidly because of their low cost, ultrastability, and high-quality imaging [2,3].

To date, DMD-based IR scene projectors have found numerous applications in the near-IR (0.76–1.6 μm) and mid-IR (3–5 μm) ranges [3–11]. However, DMD-based scene projection in the long-wave IR (8–12 μm) is hampered by the diffraction characteristics of the DMD, which results in poor image contrast and the concomitant poor image quality. Although the diffraction analysis of the DMD has been investigated by several researchers [5–7,12], contrast degradation of DMD-based scene projectors in the long-wave IR is still unsolved. In this study, the DMD is employed as a two-dimensional diffraction grating, and a numerical model of the diffraction of DMDs is constructed with the Fourier transform. Furthermore, we simulate the diffraction efficiency with MATLAB, and the simulation results are verified with an experiment in the laboratory. The simulation and experimental results provide a method to improve the contrast of DMD-based scene projectors in the long-wave IR.

2. STRUCTURE AND OPERATION OF THE DMD

The structure diagram of the DMD is presented in Fig. 1. The DMD consists of a matrix of 1024×768 micromirrors. The size of each micromirror is $a \times a$ ($13.68\ \mu m \times 13.68\ \mu m$). The micromirror pitch b is less than 1 μm. The DMD is used as a reflected spatial light modulator in DMD-based IR scene projectors. The operation principle of the DMD is depicted in Fig. 2. Each micromirror is operated in the working state, namely, the on state and the off state. In the working state, each micromirror is rotated to either +12° (on state) or −12° (off state) from the flat state [5,7]. When micromirrors are rotated at +12° (−12°), the reflected light is steered into (out of) the projection aperture. Thus, the DMD is used as a photoelectric switch, and the images are produced with gray-scale modulation by rotating the micromirrors to the on (off) state [12].

3. DIFFRACTION ANALYSIS OF THE DMD

A. Diffraction Model of a Single Micromirror [5,7]

In accordance with the structure and operating principle of the DMD, each micromirror of the DMD is used as a reflected

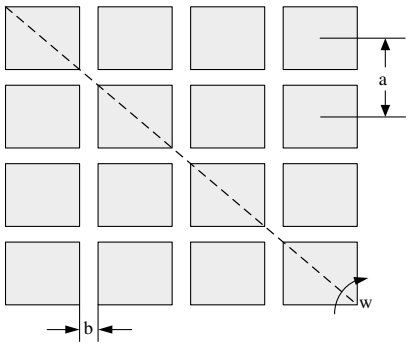

Fig. 1. Structure view of a DMD.

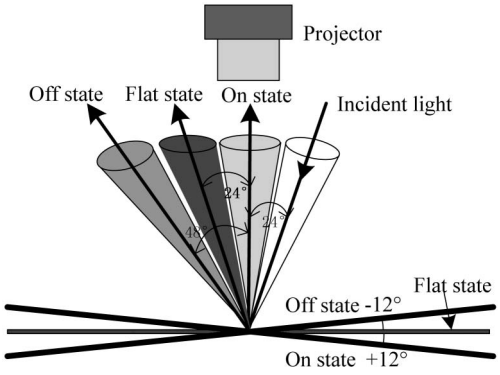

Fig. 2. Operating principle of a DMD.

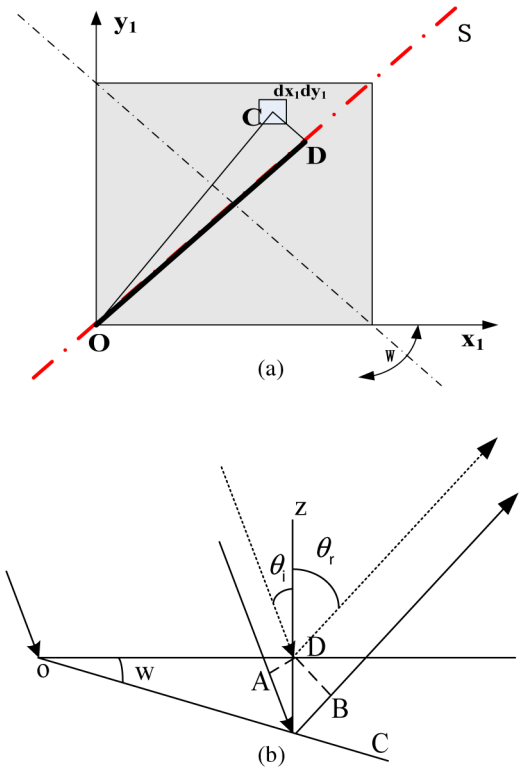

Fig. 3. (a) Diagram of a single micromirror. (b) Cross profile of a single micromirror along OS.

spatial light switch. The reflectivity of each micromirror is set to one and the effective reflection area is $a \times a$. The coordinate system of a single micromirror is established, as shown in Fig. 3. When a micromirror is in the flat state, it can be described as a rectangular function, which is defined as $\mathrm{rect}(\frac{x_1}{a})\mathrm{rect}(\frac{y_1}{a})$. When a micromirror is in the working state, it rotates $w(\pm 12°)$ along the diagonal. A phase difference is observed between the flat state and the working state. This phase difference affects the location of the diffraction order. Thus, a micromirror under the working state is defined as a rectangular function with a phase term. Figure 3(a) shows the diagram of a single micromirror. The phase term is calculated with an infinitesimal method. We take an arbitrary small element dx_1dy_1 as an example. The direction of the incident light is along the diagonal direction OS, which is the diagonal shown in Fig. 3(a). Considering that no phase difference is observed among the small elements in a counter-diagonal direction, the phase difference between dx_1dy_1 and O can be calculated along the diagonal. Figure 3(b) shows the cross profile of a single micromirror along the diagonal OS. The phase difference is expressed as follows:

$$\Phi = K\Delta = \frac{\sqrt{2}\pi}{\lambda} \tan w(\cos\theta_i + \cos\theta_r)(x_1 + y_1), \quad (1)$$

where Φ is the phase difference, $K = 2\pi/\lambda$, Δ is the optical path difference, λ is the incident wavelength, θ_i is the incident zenith angle between the incident direction of the beam and the normal direction of the DMD (z direction), and θ_r is the diffracted zenith angle between the diffraction direction of the beam and the normal direction of the DMD. Considering the phase difference Φ, the micromirror under the working state can be defined as follows:

$$\begin{aligned} r(x1, y1) &= \mathrm{rect}\left(\frac{x1}{a}\right)\mathrm{rect}\left(\frac{y1}{a}\right)e^{i\phi} \\ &= \mathrm{rect}\left(\frac{x1}{a}\right)\mathrm{rect}\left(\frac{y1}{a}\right)e^{i\sqrt{2}\pi\xi(x1+y1)}, \end{aligned} \quad (2)$$

where $\xi = \frac{1}{\lambda} \tan w(\cos\theta_i + \cos\theta_r)$.

B. Diffraction Model of the DMD

As depicted in Fig. 4, the position of each micromirror can be acquired through coordinate transformation of the micromirror in the origin. (m, n) is the number of each micromirror, and M and N are the total micromirrors along the x_1 and y_1 directions, respectively. The reflection function of an arbitrary micromirror can be expressed as follows:

$$\begin{aligned} r_{m,n}(x_1, y_1) &= \mathrm{rect}\left(\frac{x_1}{a}\right)\mathrm{rect}\left(\frac{y_1}{a}\right)e^{i\phi} \otimes \delta(x_1 - ma) \\ &\otimes \delta(y_1 - na). \end{aligned} \quad (3)$$

The entire reflection equation of the DMD is presented as follows:

$$\begin{aligned} R(x_1, y_1) &= r_{0,0} + r_{1,0} + r_{0,1} + r_{1,1} + \ldots + r_{\mathrm{M,N}} \\ &= \mathrm{rect}\left(\frac{x_1}{a}\right)\mathrm{rect}\left(\frac{y_1}{a}\right)e^{i\sqrt{2}\pi\xi(x_1+y_1)} \\ &\otimes \sum_{m=0}^{M}\delta(x_1 - ma) \otimes \sum_{n=0}^{N}\delta(y_1 - na). \end{aligned} \quad (4)$$

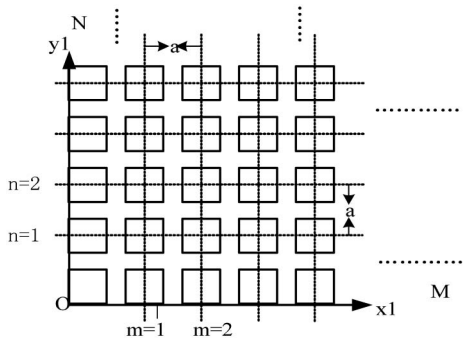

Fig. 4. Schematic plan of a DMD.

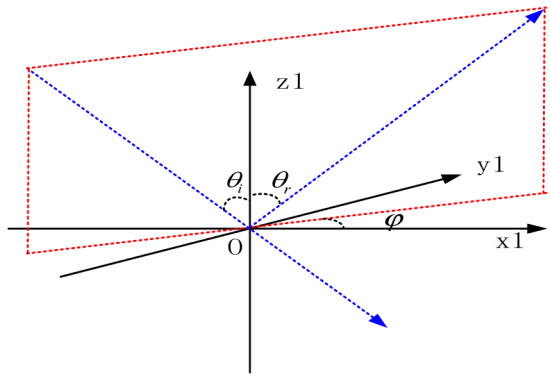

Fig. 5. Illumination source with an arbitrary incident angle.

C. Expression of Illumination Source Function

For simplicity, we assume the illumination source as a monochromatic plane wave with an amplitude of one. As depicted in Fig. 5, φ_i is the incident azimuth angle between the incident plane and the $x1oy1$ plane. θ_i is the incident zenith angle between the incident direction and the z axis. The normal vector of the incident wave can be written as $(\sin\theta_i\cos\varphi_i, \sin\theta_i\sin\varphi_i, -\cos\theta_i)$. Thus, the illumination function is expressed as follows:

$$e(x_1,y_1) = e^{i\vec{K}\bullet\vec{r}} = e^{i2\pi\left[\frac{\sin\theta_i\cos\phi_i}{\lambda}x_1+\frac{\sin\theta_i\sin\phi_i}{\lambda}y_1\right]}, \tag{5}$$

assuming $u_0 = \frac{\sin\theta_i\cos\varphi_i}{\lambda}$, and $v_0 = \frac{\sin\theta_i\sin\varphi_i}{\lambda}$. The illumination function is presented as follows:

$$e(x_1,y_1) = e^{i2\pi(u_0x_1+v_0y_1)}. \tag{6}$$

D. Diffraction Intensity Distribution of the DMD

Combining the reflection in Eq. (4) with the illumination function in Eq. (6), the distribution of the complex amplitude of the incident wave is expressed as follows:

$$\begin{aligned} U(x_1,y_1) &= R(x_1,y_1)e(x_1,y_1) \\ &= \left\{\text{rect}\left(\frac{x_1}{a}\right)\text{rect}\left(\frac{y_1}{a}\right)e^{i\sqrt{2}\pi\xi(x_1+y_1)}\right. \\ &\quad\otimes\sum_{m=0}^{M}\delta(x_1-ma) \\ &\quad\left.\otimes\sum_{n=0}^{N}\delta(y_1-na)\right\}e^{i2\pi(u_0x_1+v_0y_1)}. \end{aligned} \tag{7}$$

Equation (7) is the Fourier transform, and the distribution of the complex amplitude of diffraction wave is presented as follows:

$$\begin{aligned} U(x_2,y_2) &= cF\{U(x1,y1)\} \\ &= ca^2\sin c\left[a\left(u-\frac{\xi}{\sqrt{2}}-u_0\right)\right]\sin c\left[a\left(v-\frac{\xi}{\sqrt{2}}-v_0\right)\right] \\ &\quad\times e^{-i\frac{M}{2}\delta}\frac{\sin\left(\frac{M+1}{2}\delta\right)}{\sin\left(\frac{\delta}{2}\right)}e^{-i\frac{N}{2}\epsilon}\frac{\sin\left(\frac{N+1}{2}\epsilon\right)}{\sin\left(\frac{\epsilon}{2}\right)}. \end{aligned} \tag{8}$$

So, the diffraction intensity distribution of the DMD can be written as

$$\begin{aligned} &I(x_2,y_2) \\ &= I_0\sin c^2\left[a\left(u-\frac{\xi}{\sqrt{2}}-u_0\right)\right]\sin c^2\left[a\left(v-\frac{\xi}{\sqrt{2}}-v_0\right)\right] \\ &\quad\times\left|\frac{\sin[\pi a(M+1)(u-u_0)]}{\sin[\pi a(u-u_0)]}\right|^2\left|\frac{\sin[\pi a(N+1)(v-v_0)]}{\sin[\pi a(v-v_0)]}\right|^2, \end{aligned} \tag{9}$$

where I_0 is the intensity coefficient, $u = \frac{\sin\theta_r\cos\varphi_r}{\lambda}$, $u_0 = \frac{\sin\theta_i\cos\varphi_i}{\lambda}$, $v = \frac{\sin\theta_r\sin\varphi_r}{\lambda}$, $v_0 = \frac{\sin\theta_i\sin\varphi_i}{\lambda}$ and $\xi = \frac{1}{\lambda}\tan w(\cos\theta_i+\cos\theta_r)$.

E. Diffraction Order and Diffraction Efficiency of the DMD

As described previously, the DMD is treated as a two-dimensional diffraction grating. The grating equation is expressed as follows [13,14]:

$$\begin{aligned} u-u_0 &= \frac{\sin\theta_r\cos\phi_r}{\lambda}-\frac{\sin\theta_i\cos\phi_i}{\lambda} = \frac{p}{a}, \\ v-v_0 &= \frac{\sin\theta_r\sin\phi_r}{\lambda}-\frac{\sin\theta_i\sin\phi_i}{\lambda} = \frac{q}{a}, \end{aligned} \tag{10}$$

where (p, q) is the diffraction order. p and q should be integers. Thus, the diffraction intensity distribution of the diffraction order is derived as follows:

$$I_{(m,n)} = I'\sin c^2\left[a\left(\frac{p}{a}-\frac{\xi}{\sqrt{2}}\right)\right]\sin c^2\left[a\left(\frac{q}{a}-\frac{\xi}{\sqrt{2}}\right)\right], \tag{11}$$

where $I' = (M+1)^2(N+1)^2I_0$. The diffraction efficiency of the DMD can be determined as follows:

$$\eta = \frac{I_{(p,q)}}{I'} = \sin c^2\left[a\left(\frac{p}{a}-\frac{\xi}{\sqrt{2}}\right)\right]\sin c^2\left[a\left(\frac{q}{a}-\frac{\xi}{\sqrt{2}}\right)\right]. \tag{12}$$

4. SIMULATION ANALYSIS OF THE DIFFRACTION MODEL

A. Simulation Result Analysis

The diffraction grating model of the DMD is developed in Section 3 with scalar diffraction and the Fourier transform.

In this study, we use MATLAB to implement a simulation of the diffraction model. The quantitative calculations of the diffraction efficiency are given. The parameters of the grating model are as follows: incident wavelength λ: 8–12 μm, incident zenith angle θ_i: 0°–90°, and incident azimuth angle φ_i: 0°–90°. After inserting these parameters into Eq. (10), the simulation results are explained further.

The simulation results we list in Tables 1 and 2 are only for a few representative incident angles, with an incident wavelength of 10 μm to facilitate the description. A three-dimensional (3D) plot of the diffraction efficiencies and angles are shown in Fig. 6. Only four diffraction orders of the DMD grating model are presented, and they are (−1, −1), (−1, 0), (0,0), and (0,1). Considering the optical layout of the DMD-based IR scene projector in Fig. 7(a), the diffraction energy from the on (off) state micromirrors should be steered into (out of) the projector system. When the micromirrors are in the on (off) state, the diffraction azimuth angle φ_r should be equal to the incident azimuth angle φ_i, and the diffraction zenith angle θ_r should be less than the aperture angle of the projector system. The DMD-based projector systems often consist of $F/2.4$–$F/3$ configurations, and the corresponding aperture angle of the projectors is between 9.4° and 11.7°. In our simulation, the F number of the projector system is 2.8. Therefore, θ_r should be less than 10.8°.

As listed in Tables 1 and 2, some conclusions can be drawn as follows:

(a) When the incident azimuth angle φ_i is 0° or 90°, the zenith angle θ_i is 36° to 50°, and the diffraction energy from the on (off) state micromirrors will be steered into (out of) the projector system.

(b) When the azimuth angle φ_i is 0° and the incident zenith angle θ_i is 48°, the diffraction efficiency with micromirrors in the on (off) state is 21% (4.8%).

(c) When the azimuth angle φ_i is 90° and the incident zenith angle θ_i is 48°, the diffraction efficiency with micromirrors in the on (off) state is 16% (4.6%). Detailed results of the simulation show that the diffraction efficiency with micromirrors in the on (off) state is approximately 20% (4%) when the incident azimuth angle φ_i is 0° or 90°, and the zenith angle θ_i is between 38° and 50°.

B. Contrast Analysis of the DMD-based Scene Projector

The contrast of the DMD-based scene projector is defined as follows [7,12]:

$$C = \frac{I_{\text{on}} - I_{\text{off}}}{I_{\text{on}} + I_{\text{off}}}, \tag{13}$$

where C is the contrast, and $I_{\text{on}}(I_{\text{off}})$ is the diffraction intensity steered into the projector with micromirrors in the on (off) state. By inserting the simulation results of Section 4.A into Eq. (13), the contrast of the DMD-based scene projectors for various incident angles is obtained. The contrast we list in Table 3 is only for a few representative incident angles to facilitate the description.

We can conclude that, when the incident zenith angle θ_i is the same, the contrast with a 0° azimuth angle is better than that with a 90° azimuth angle. Furthermore, when the incident azimuth angle is 0° and the zenith angle is 42° to 46°, the projector can obtain the best contrast of approximately 0.7.

Table 1. Diffraction Angles and Efficiencies at $\lambda = 10\ \mu$m with All Micromirrors in the On State

	Diffraction Angles (ϕ_r,θ_r) and Efficiencies (η) for Different Orders			
Incident Angle (ϕ_i,θ_i)	**(−1, − 1)**	**(−1,0)**	**(0, − 1)**	**(0,0)**
(0°, 24°)	(66°, 53°; 3%)	(0°, −19°; 22%)	(−61°, 57°; 15%)	(0°, 24°; 60%)
(0°, 36°)	(79°, −48°; 4%)	(0°, 8.8°; 23%)	(−51°, 70°; 9%)	(0°, 36°; 64%)
(0°, 48°)	(−89°, 47°; 2%)	(0°, 0°; 21%)	(—,—; —)	(0°, 48°; 77%)
(45°, 24°)	(45°, −39°; 6%)	(−33°, −32°; 19%)	(−57°, 32°; 19%)	(45°, 24°; 56%)
(45°, 36°)	(45°, −27°; 4%)	(−53°, −31°; 16%)	(−37°, 31°; 16%)	(45°, 36°; 64%)
(45°, 48°)	(45°, −17°; 4%)	(−69°, −34°; 12%)	(−21°, 34°; 12%)	(45°, 48°; 72%)
(90°, 24°)	(24°, −53°; 3%)	(−29°, −57°; 16%)	(−90°, 19°; 22%)	(90°, 24°; 59%)
(90°, 36°)	(11°, −48°; 3%)	(−39°, −70°; 10%)	(−90°, 8°; 19%)	(90°, 36°; 68%)
(90°, 48°)	(−1°, −47°; 1%)	(—,—; —)	(90°, 1°; 16%)	(90°, 48°; 82%)

Table 2. Diffraction Angles and Efficiencies at $\lambda = 10\ \mu$m with All Micromirrors in the Off State

	Diffraction Angles (ϕ_r,θ_r) and Efficiencies (η) for Different Orders			
Incident Angle (ϕ_i,θ_i)	**(−1, − 1)**	**(−1,0)**	**(0, − 1)**	**(0,0)**
(0°, 24°)	(66°, −53°; 1%)	(0°, −19°; 7%)	(−61°, 57°; 6%)	(0°, 24°; 86%)
(0°, 36°)	(79°, −48°; 0.5%)	(0°, 8.8°; 6%)	(−51°, 70°; 5.5%)	(0°, 36°; 88%)
(0°, 48°)	(−89°, 47°; 0.2%)	(0°, 0°; 4.8%)	(—,—; —)	(0°, 48°; 95%)
(45°, 24°)	(45°, −39°; 0.5%)	(−33°, −32°; 6.8%)	(57°, 32°; 6.7%)	(45°, 24°; 86%)
(45°, 36°)	(45°, −27°; 0.4%)	(−53°, −31°; 5.6%)	(−37°, 31°; 6%)	(45°, 36°; 88%)
(45°, 48°)	(45°, −17°; 0.3%)	(−69°, −34°; 4.5%)	(−21°, 34°; 5.2%)	(45°, 48°; 90%)
(90°, 24°)	(24°, −53°; 0.5%)	(−29°, −57°; 6.8%)	(−90°, 19°; 6.7%)	(90°, 24°; 86%)
(90°, 36°)	(11°, −48°; 0.3%)	(−39°, −70°; 5.4%)	(−90°, 8°; 6.3%)	(90°, 36°; 88%)
(90°, 48°)	(−1°, −47°; 0.4%)	(—,—; —)	(90°, 1°; 4.6%)	(90°, 48°; 95%)

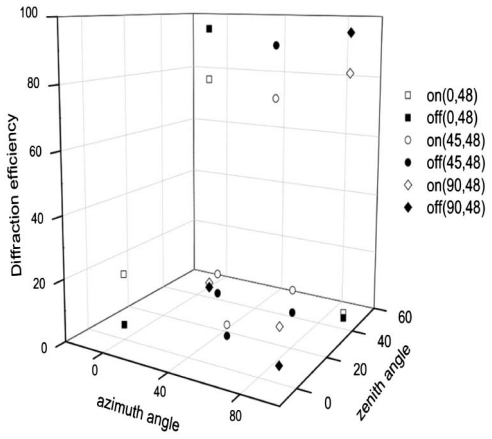

Fig. 6. 3D plot of diffraction efficiencies and angles at $\lambda = 10$ μm.

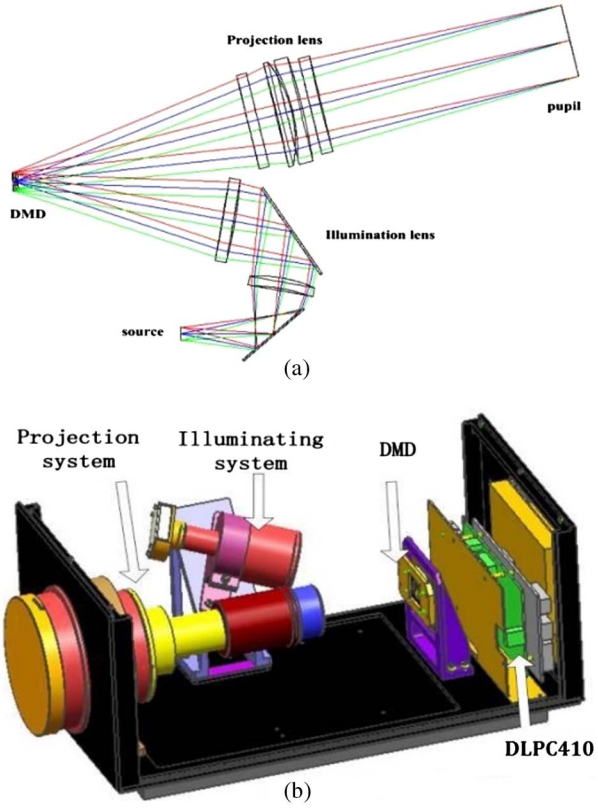

Fig. 7. System structure of a DMD-based IR scene projector.

5. EXPERIMENTAL VERIFICATION

A series of experiments were conducted to further verify the simulation analysis presented previously. Figure 7 shows the system of the DMD-based IR scene projector that we developed.

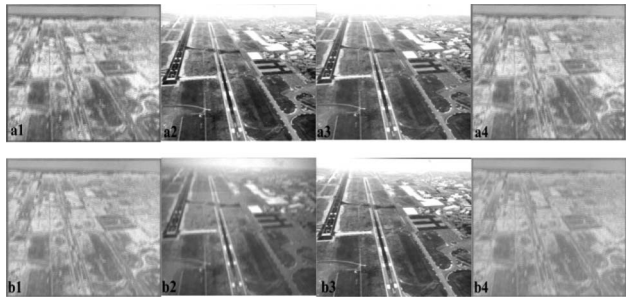

Fig. 8. IR images with different incident angles (ϕ_i, θ_i): a1(0°, 38°), a2(0°, 42°), a3(0°, 46°), a4(0°, 50°), b1(90°, 38°), b2(90°, 42°), b3(90°, 46°), and b4(90°, 50°).

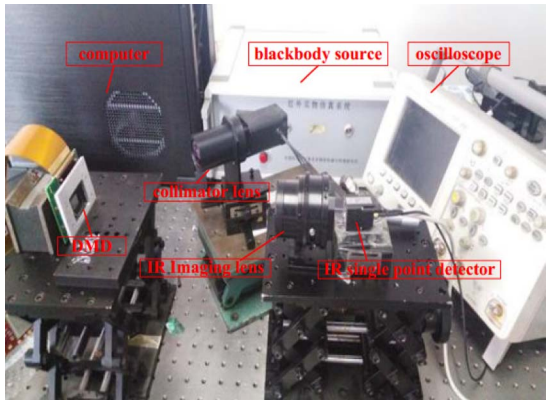

Fig. 9. Experimental system for the contrast measurement of IR images.

Figure 7(a) is the optical layout, which is composed of a source, an illumination lens, a DMD, and a projection lens. In the system design, a blackbody is often the preferred. The illumination system adopts the Kohler illumination and consists of four germanium lenses. The projection system adopts a telecentric optical structure and consists of four lenses. The glass material is Ge and ZnS.

Figure 7(b) is the mechanical structure of the projector system. The projector system consists of an $F/2.8$ configuration. We verify the simulation results in the IR scene simulation system with this DMD-based scene projector. The contrast of the DMD-based scene projector with different incident angles is discussed in detail.

In this section, the projector system generated IR images at an incident azimuth angle of 0° (90°) and a zenith angle of 38° to 50°. Figure 8 shows the experimental results which are aerial IR images. Figure 8(a) shows the IR images generated at an incident azimuth angle of 0°. Figure 8(b) shows the IR images generated at an incident azimuth angle of 90°.

Table 3. Contrast of DMD-based Scene Projector System at $\lambda = 10$ μm with Different Incident Angles

Incident Angle (ϕ_i, θ_i)	(0°, 38°)	(0°, 42°)	(0°, 46°)	(0°, 50°)	(90°, 38°)	(90°, 42°)	(90°, 46°)	(90°, 50°)
Projector Contrast (C)	0.51	0.70	0.74	0.52	0.48	0.62	0.66	0.42

Table 4. Contrast of Aerial IR Images with Different Incident Angles

Incident Angle (ϕ_i, θ_i)	(0°, 38°)	(0°, 42°)	(0°, 46°)	(0°, 50°)	(90°, 38°)	(90°, 42°)	(90°, 46°)	(90°, 50°)
Projector Contrast (C)	0.52	0.65	0.71	0.48	0.44	0.63	0.68	0.41

To verify the simulation results, an experiment for the contrast measurement of IR images has been done. The experimental system is shown in Fig. 9, which consists of a computer, a blackbody source, collimator lenses, a DMD, IR imaging lenses, an IR detector, and an oscilloscope. The results are shown in Table 4. As shown in Table 4, the contrast of the projector with a 0° incident azimuth angle is better than that with 90°, which agrees well with the simulation results. At the same time, when the incident zenith angle is 42° to 46°, the contrast of the projector is better than 0.6. The experiment is consistent with the simulation results. As can be concluded, the diffraction grating model established in Section 3 is able to analyze the diffraction of the DMD-based scene projector in the long-wave IR.

6. CONCLUSIONS

In this study, the diffraction analysis of a DMD-based scene projector in the long-wave IR has been presented in detail. We have developed diffraction grating models of the DMD based on the scalar diffraction theory and the Fourier transform. Simulations and experiments are conducted to analyze and calculate the diffraction characteristic of the grating model. The results indicate that when the incident azimuth angle is 0° and the zenith angle is 42° to 46°, the projector will acquire the best contrast. The diffraction grating model proposed in this study is available for a series of DMD-based scene projectors in the long-wave IR. Furthermore, from the simulation in Section 4.B, the diffraction efficiency of the DMD in the long-wave is approximately 20%. How to improve the diffraction efficiency of the DMD in the long-wave IR is what we will solve in future work.

Funding. National Key Scientific Instrument and Equipment Development Project (2013YQ140517); Changchun Science and Technology Program Key Projects (14KG011).

REFERENCES

1. L. Zhang, Y. Tian, and Q. Li, "Research status and prospect of dynamic infrared scene projector," Inf. Laser Eng. **41**, 1423–1431 (2012).
2. Y. Sun, F. Long, and Q. Meng, "Infrared target simulator's polarizing beamsplitter system based on digital-micromirror device," Inf. Laser Eng. **43**, 749–753 (2012).
3. X. Quan, H. Liu, and Z. Lu, "Correction and analysis of noise in Hadamard transform spectrometer with digital micro-mirror device and double sub-gratings," Opt. Commun. **359**, 95–101 (2016).
4. J. Zhang, *Study on the Optical System of an Infrared Dual-band Scene Simulator* (Changchun Institute of Optics, Fine Mechanics and Physics, Chinese Academy of Sciences, 2013).
5. Z. Xiong, H. Liu, and X. Q. Tan, "Diffraction analysis of digital micromirror device in maskless photolithography system," J. Micro/Nanolith. MEMS MOEMS **13**, 043016 (2014).
6. J. R. Dupuis and D. Mansur, "Considerations for DMDs operating in the infrared," Proc. SPIE **8254**, 82540J (2012).
7. K. J. Barnard, G. D. Boreman, and D. R. Pape, "Crosstalk model of a deformable-mirror-based infrared scene projector," Opt. Eng. **33**, 140–149 (1994).
8. J. R. Dupuis, D. Mansur, and R. Vaillancourt, "High-dynamic range DMD-based IR scene projector," Proc. SPIE **8618**, 86180R (2013).
9. D. Dudley, W. M. Duncan, and J. Slaughter, "Emerging digital micromirror device (DMD) applications," Proc. SPIE **4985**, 14–25 (2003).
10. J. P. Rice, "DMD diffraction measurements to support design of projectors for test and evaluation of multispectral and hyperspectral imaging sensors," Proc. SPIE **7210**, 72100D (2009).
11. F. Y. Xu, Y. Li, and Z. Q. Gao, "Diffraction characteristics of DMD and its applications in holographic display," Acta Photon. Sin. **40**, 332–336 (2011).
12. Y. Meuret and P. De Visschere, "Contrast-improving methods for digital micro-mirror device projectors," Opt. Eng. **42**, 840–845 (2003).
13. M. H. Hutley, *Diffraction Gratings* (Academic, 1982), pp. 36–38.
14. D. C. O'Shea, *Elements of Modern Optical Design* (Wiley, 1985), pp. 327–328.